Supplementary Information

Detection of Copper (II) and Aluminium (III) by a new bis-benzimidazole Schiff base in aqueous media *via* distinct routes

Ashish Kumar, Amit Kumar, Mrigendra Dubey, Arnab Biswas and Daya Shankar Pandey*

Department of Chemistry, Faculty of Science, Banaras Hindu University, Varanasi - 221 005 (U.P.), India

Table of Contents: **Pages**

Experimental details:

General procedures. Elemental analyses on samples were performed in the Micro Analytical Laboratory of SAIF, Central Drug Research Institute (CDRI) Lucknow. IR and UV/vis spectra were acquired on PerkinElmer Spectrum Version 10.03.05 FT-IR and Shimadzu UV-1601 spectrophotometers, respectively. ^{1}H (300 MHz) and ^{13}C (75.45 MHz) NMR spectra were acquired at room temperature (rt) on a JEOL AL300 FT-NMR spectrometer using tetra-methylsilane [$Si(CH_3)_4$] as an internal reference. Fluorescence spectra were obtained in methanol water mixture ($MeOH/H_2O$, 9:1, v/v) on a PerkinElmer *LS-55* Fluorescence Spectrometer at rt. Electrospray ionization mass spectrometric (ESI-MS) measurements were made on a THERMO Finningan LCQ Advantage Max ion–trap mass spectrometer. Limit of detection (LOD) were evaluated using linear calibration plots of quantitative fluorescence response for **H_3L** vs. Cu^{2+} and Al^{3+} (for the band at 485 and 466 nm, respectively). It has been calculated as $3\sigma/s$, where σ is the standard deviation of the blank signal and '*s*' is the slope of corresponding linear calibration plot. Quantum chemical calculations have been performed using a hybrid version of DFT method, namely B3LYP.[1] Basis set 6-31G** was used for C, H, N and O, while LANL2DZ for Cu and Al which combines quasi-relativistic effective core potentials with a valence double basis-set.[2] Geometry optimization and frequency calculations (to verify a genuine minimum energy structure) for **H_3L**, complex **1** and **2** were performed using Gaussian 09 programme.[3]

UV/vis and fluorescence studies. Stock solution of **BBA** and **H_3L** (1.0×10^{-3} M) were prepared in $MeOH/H_2O$ (9:1; v/v) and their diluted solutions were used for UV/vis and fluorescence studies. Stock solutions of various metal ions *viz*. Na^+, K^+, Mg^{2+}, Ca^{2+}, Fe^{3+}, Mn^{2+}, Co^{2+}, Ni^{2+}, Cu^{2+}, Ag^+, Zn^{2+}, Cd^{2+}, Hg^{2+}, Al^{3+} and Pb^{2+} (*c*, 1.0×10^{-1} M) were prepared by dissolving nitrate salts (NO_3^-) of respective metals in triply distilled water and used after required dilutions (*c*, 1.0×10^{-2} M, 1.0×10^{-3} M). In a typical UV/vis or fluorescence titration experiment, solution of **BBA**/**H_3L** was taken in a quartz cuvette (3.0 mL; path length, 1 cm) and treated gradually with dilute solution of the metal ions with the help of a micropipette. Observed spectral changes were noted as a function of equivalent of metal ions after ~1 min. of each addition and experiments were repeated thrice.

X-ray structure determinations. Crystals suitable for single crystal X–ray diffraction analyses were obtained from DCM/MeOH (v/v, 1:1) solution of **H_3L**. The crystal was

mounted on a glass fibre. All the geometric and intensity data were collected at 293 K on a Rigaku Saturn 724+ CCD diffractometer with a fine-focus sealed tube Cu-K_α (λ = 1.54184 Å) X-ray source with increasing ω (width of 0.3 per frame) at a scan speed of either 3 or 5 s/frame. After initial solution of the reflection data, refinement was performed by WinGX environment using direct methods (SHELXL 97) and full-matrix least squares on F^2 (SHELX 97).[4] All non-hydrogen atoms were refined anisotropically and hydrogen atoms geometrically fixed and refined as per the riding model. Powder X-ray diffraction data was collected on a Bruker Eco D8 Advanced X-ray diffractometer between angle 2Θ = 5–60°.

Results and discussion

Deuterium ion exchange experiment on H_3L. To investigate the interactions between benzimidazole group and Al^{3+} a hydrogen-deuterium exchange in **H_3L** (dmso-d_6) in presence of blank D_2O (only a trace amount) has been monitored through ^1H NMR experiment. The experiment displayed a feeble loss for –NH signal and a drastic loss for –OH signal after immediate addition of D_2O only. With increase in time, it has been noted that shortly after addition of D_2O, the –OH signal disappeared almost completely while the –NH signal persists over a significant period of time (~1 h, including time for scanning). This substantiates more stability of –NH than –OH under biased deuterium exchange conditions in the solution. In other words, it significantly proves the interaction between Al^{3+} and –NH of benzimidazole because, in the **H_3L** vs. Al^{3+} titration, signal for –NH was found to be disappeared prior to the signal for –OH which should not occur if deuterium exchange dominates over interaction involved with Al^{3+}. Therefore, it has been concluded from the ^1H NMR studies that drastic loss of resonance for –NH proton occurred predominantly due to the presence Al^{3+} and also that benzimidazole is more reactive towards Al^{3+}.

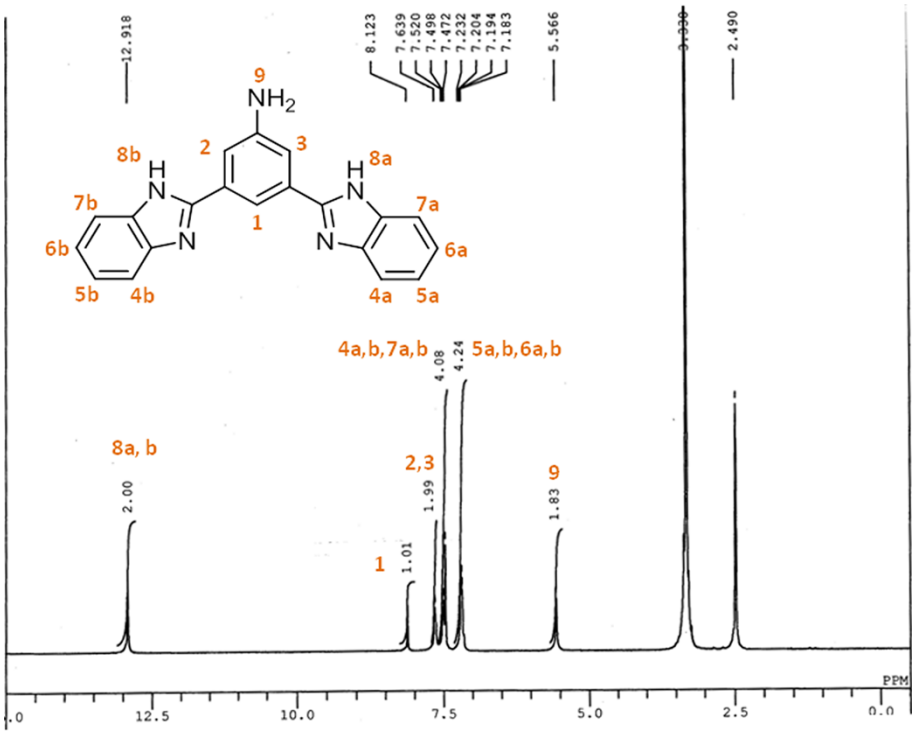

(a)

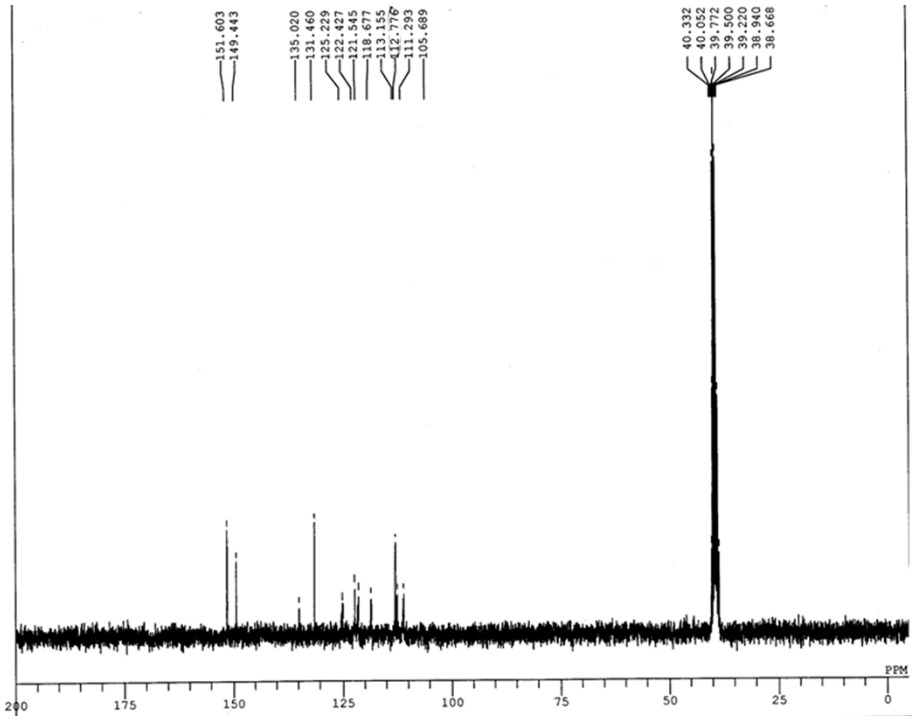

(b)

Fig. S1 (a) ^{1}H NMR and (b) ^{13}C NMR spectra of 3,5-*bis*(1H-benzimidazol-2-yl)aniline (**BBA**).

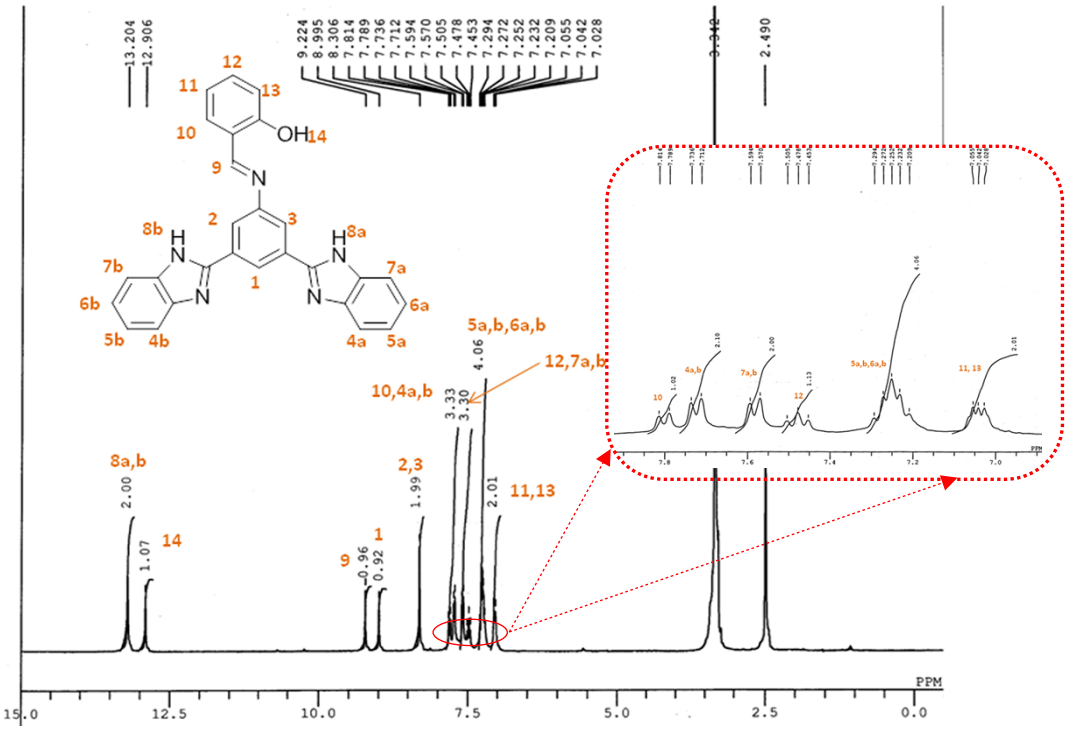

(a)

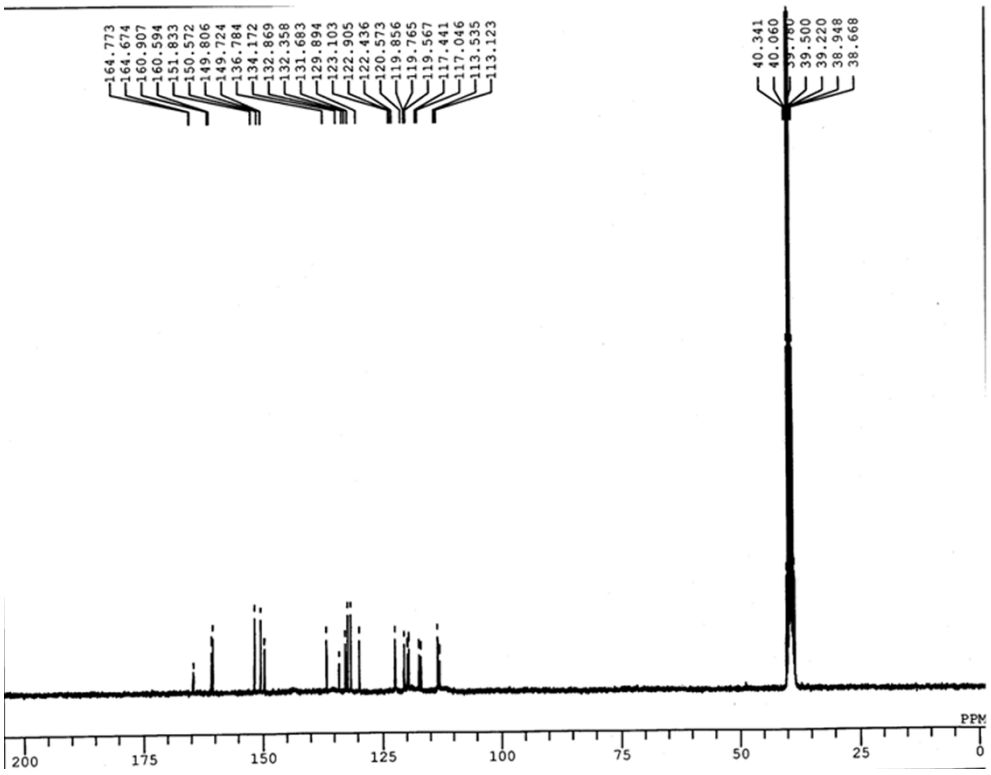

(b)

Fig. S2 (a) ^{1}H and (b) ^{13}C NMR spectrum of 2-(3,5-*bis*(1H-benzimidazol-2-yl)phenyl-imino-methyl)phenol (**H_3L**).

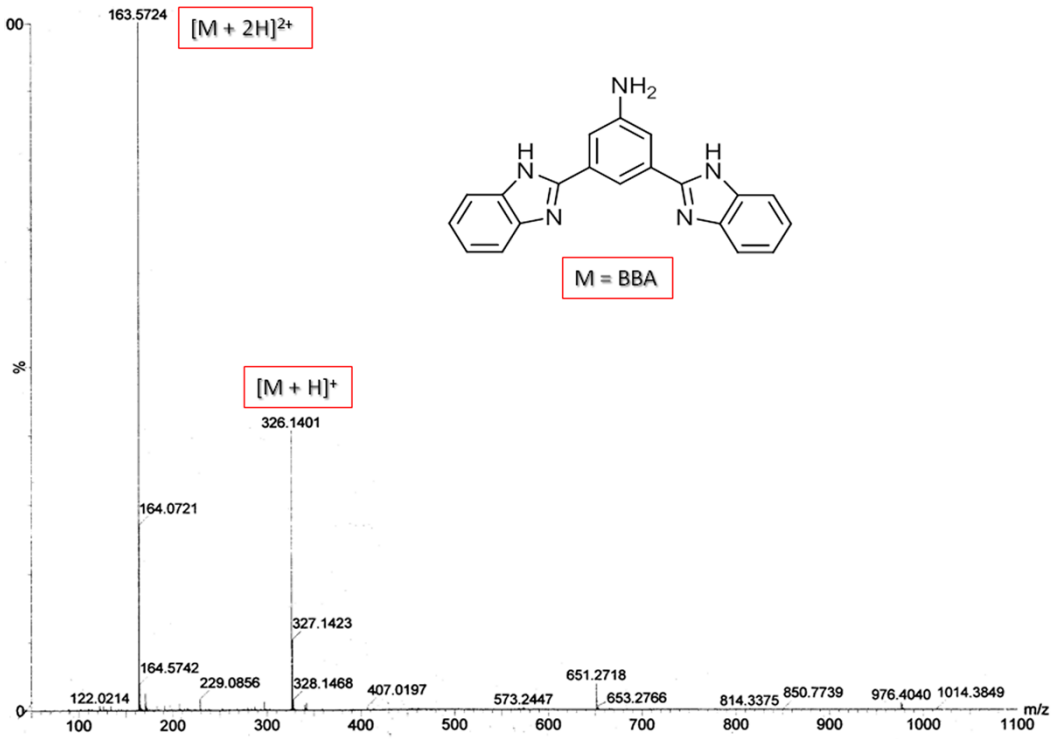

(a)

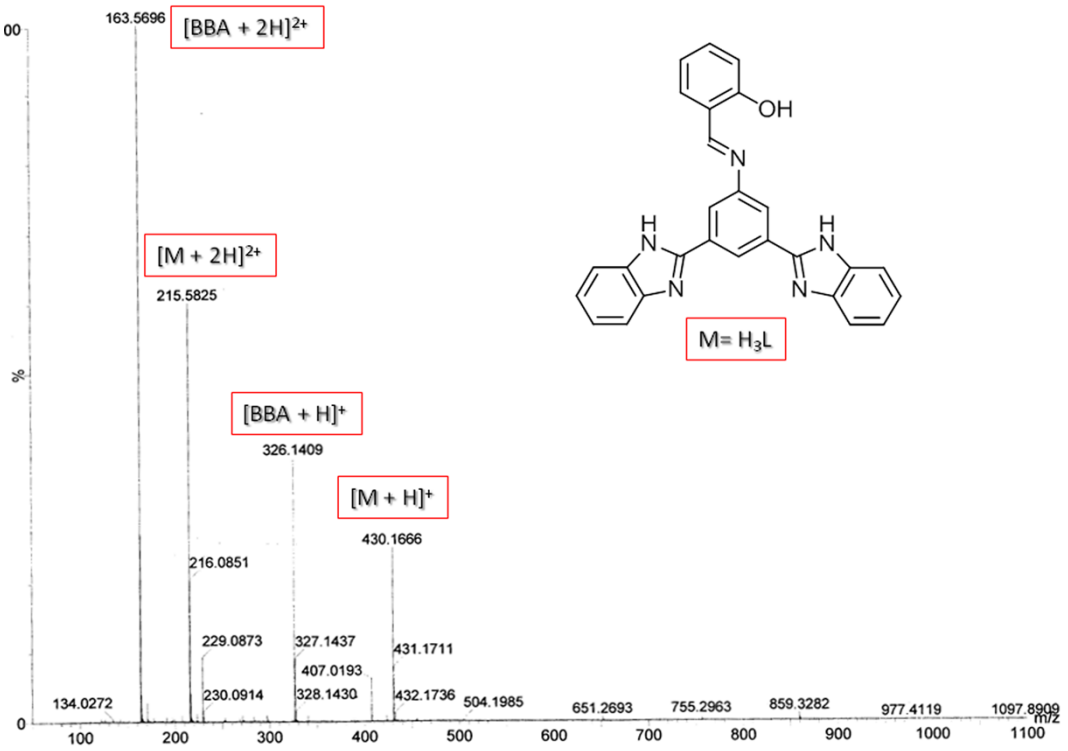

(b)

Fig. S3 (a) ESI–MS of **BBA** and (b) **H_3L**.

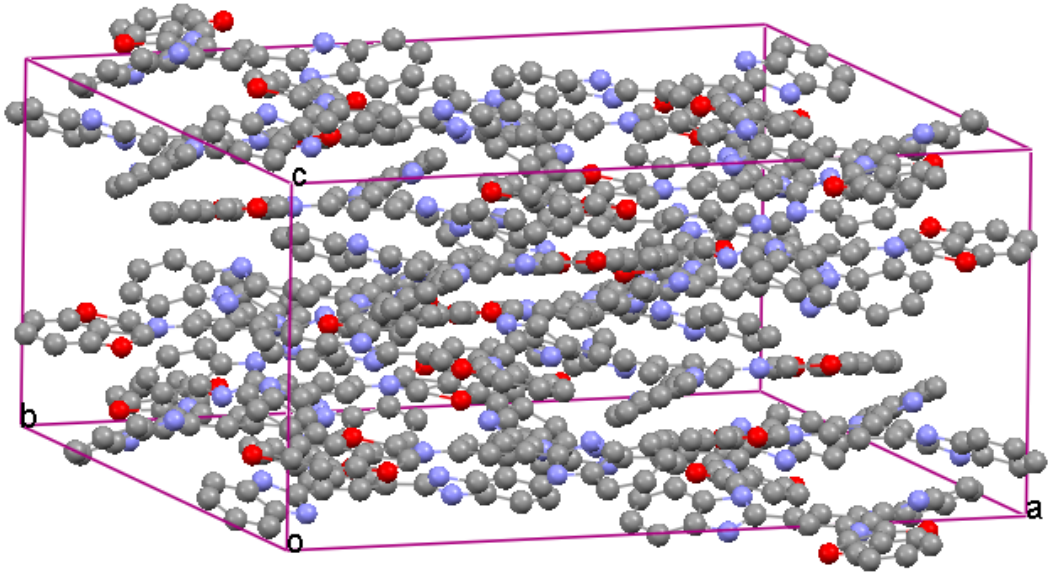

(a)

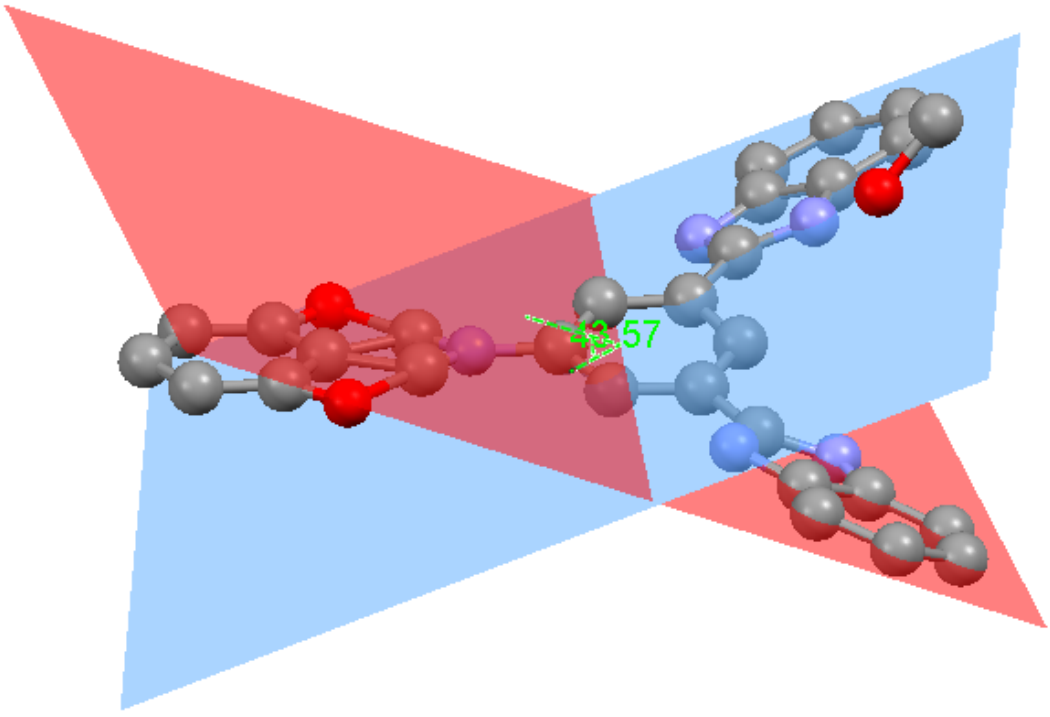

(b)

Fig. S4 (a) Crystallographic packing of **H_3L**. (a) Difference between the planes associated with both benzimidazole rings which are found to be 43.57°. This type of twisting may be a related to affect PET. (c) Extended structure of **H_3L** in crystallographic '*ab*' plane showing anti-parallel arrangement of subsequent units.

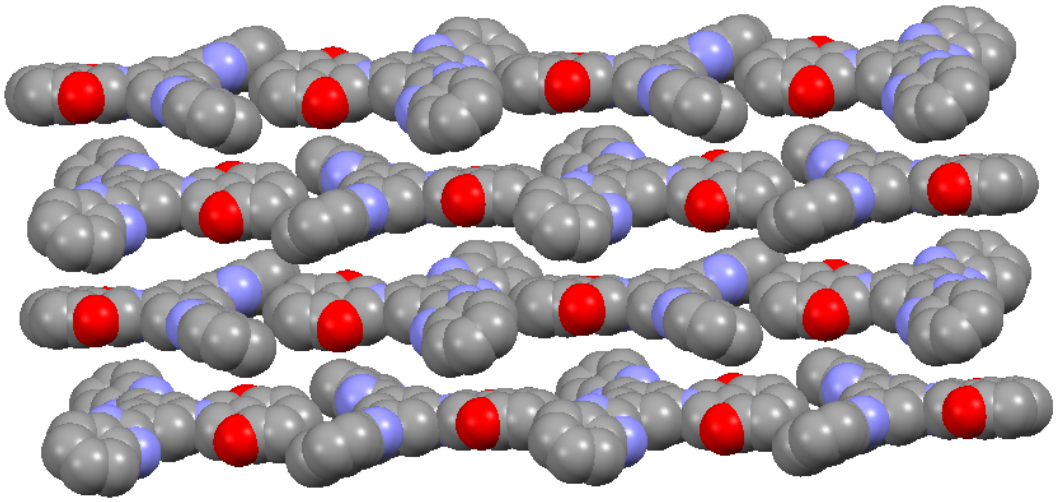

(a)

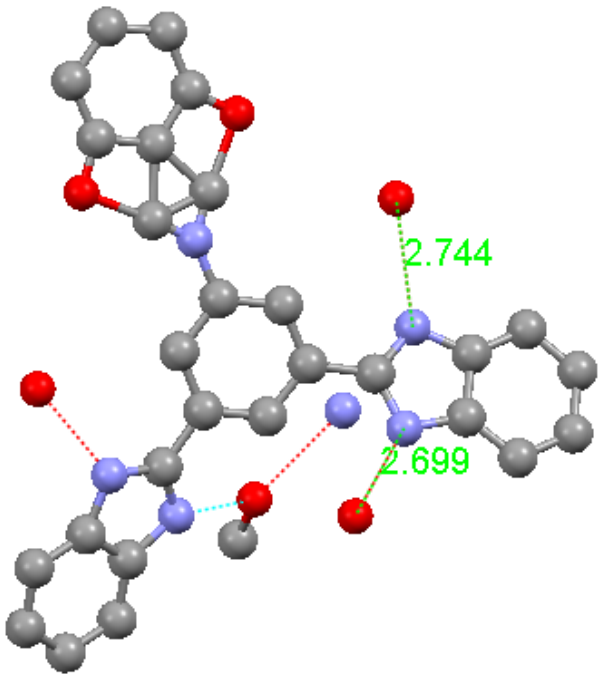

(b)

Fig. S5 (a) The anti-parallel arrangement of **H_3L** along crystallographic '*c*' axis in '*ab*' plane. (b) Hydrogen bonding interactions associated with methanol solvent molecule.

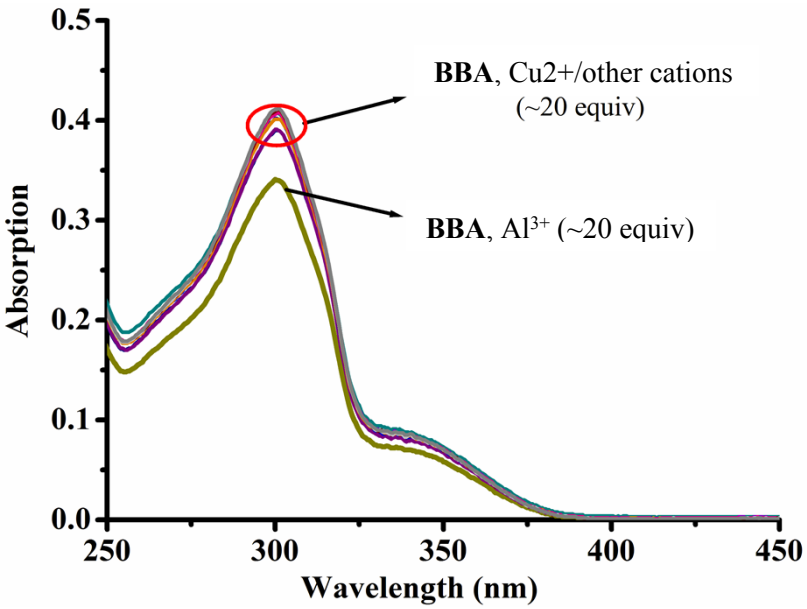

Fig. S6 (a) UV/vis spectra of **BBA** (*c*, 1.0 × 10^{-5} M; MeOH/H_2O, 9:1, v/v) only, and in presence of several metal ions. (b) UV/vis spectra showing the effect of Al^{3+} (20.0 equiv) on **BBA**. Considerably large quantity of Al^{3+} needed has been attributed towards low sensitivity.

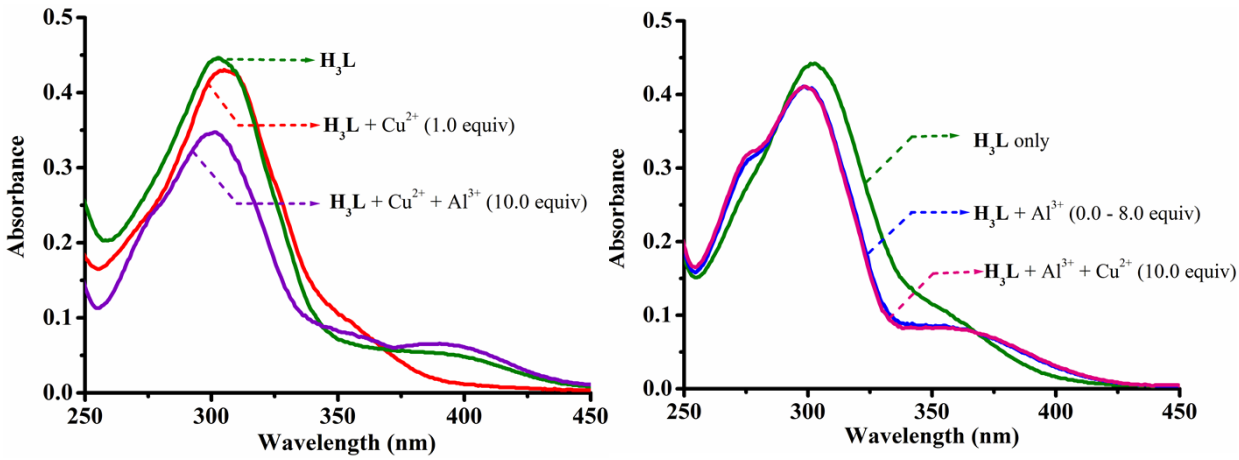

Fig. S7 UV/vis spectra of $\mathbf{H_3L}$ (*c*, 1.0 × 10^{-5} M; MeOH/H_2O, 9:1, v/v) showing mutual interference of Al^{3+} and Cu^{2+} respectively.

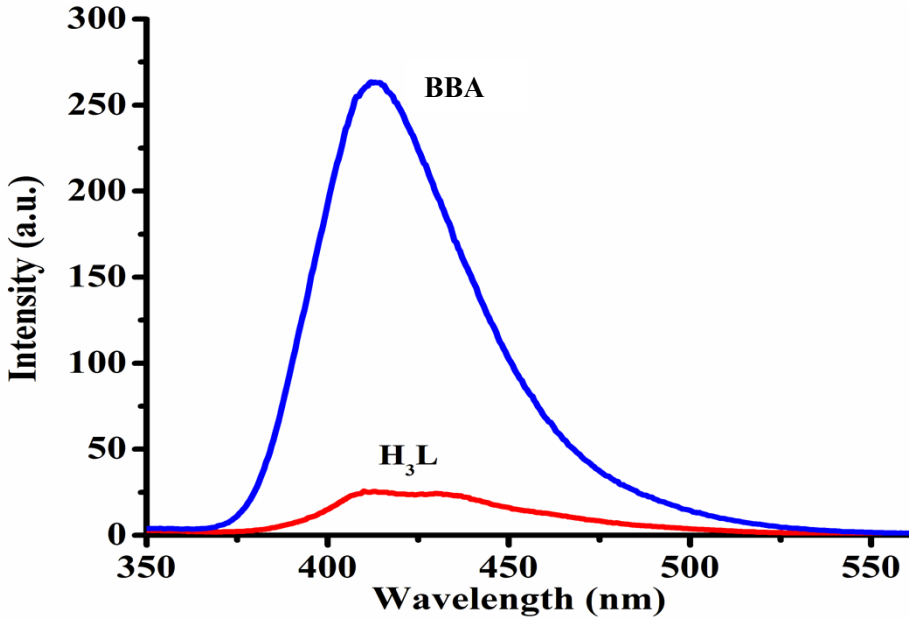

Fig. S8 Fluorescence spectra of **H_3L** and (b) **BBA** (*c*, 1.0 × 10^{-6} M; MeOH/H_2O, 9:1, v/v; *p*H ~7.2).

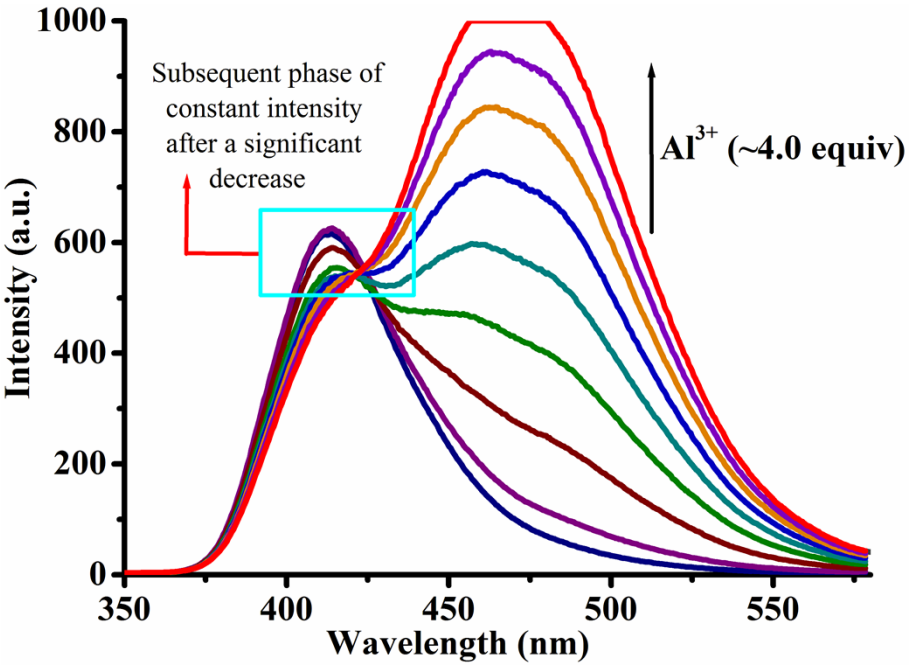

Fig. S9 Fluorescence titration spectra of **H_3L** at *c*, 1.0 × 10^{-5} M [MeOH/H_2O, 9:1, v/v] in presence of Al^{3+}. It has been performed anonymously just to show clear *binary spectral behaviour* pertaining to the involvement of benzimidazole and salen interactions in a cumulative manner.

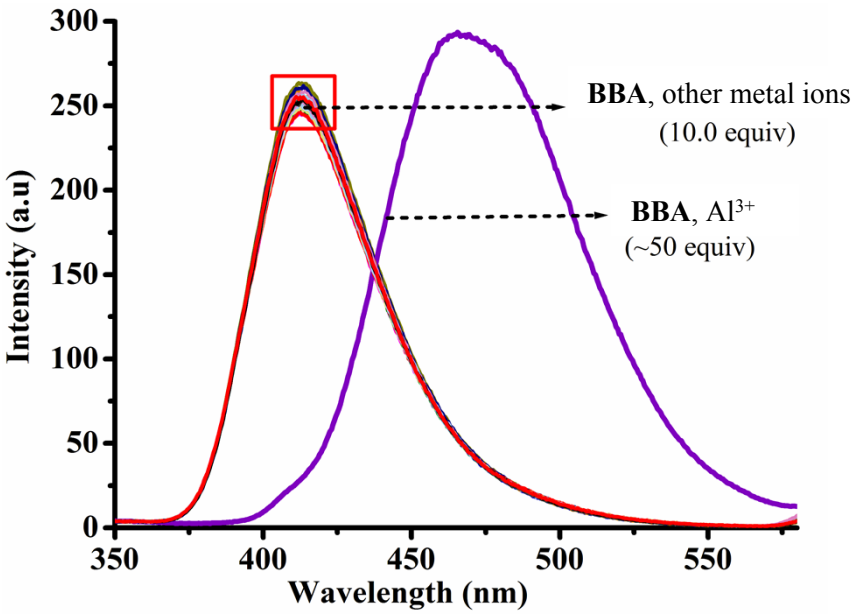

Fig. S10 Fluorescence titration spectra of **BBA** [*c*, 1.0 × 10^{-6} M; MeOH/H_2O, 9:1, v/v] only and in the presence of various metal ions (10.0 equiv). In presence of excess of Al^{3+} (~50 equiv) significant changes occurs confirming benzimidazole-Al^{3+} interactions.

(a)

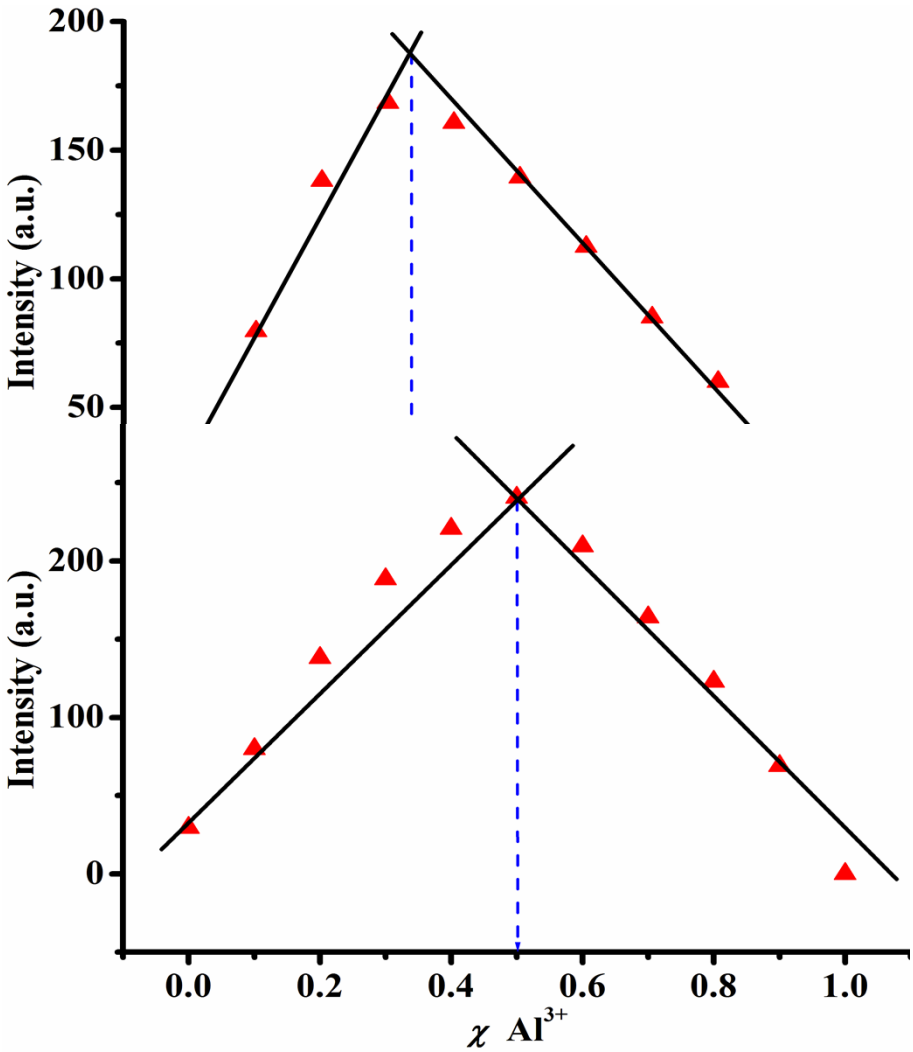

(b)

Fig. S11 Job's plot analyses for the stoichiometric determination of (a) $\mathbf{H_3L}$ + Cu^{2+} and (b) $\mathbf{H_3L}$ + Al^{3+}. Former shows 1:2 stoichiometry whereas latter exhibits 1:1 stoichiometric ratio between the probe and respective analytes.

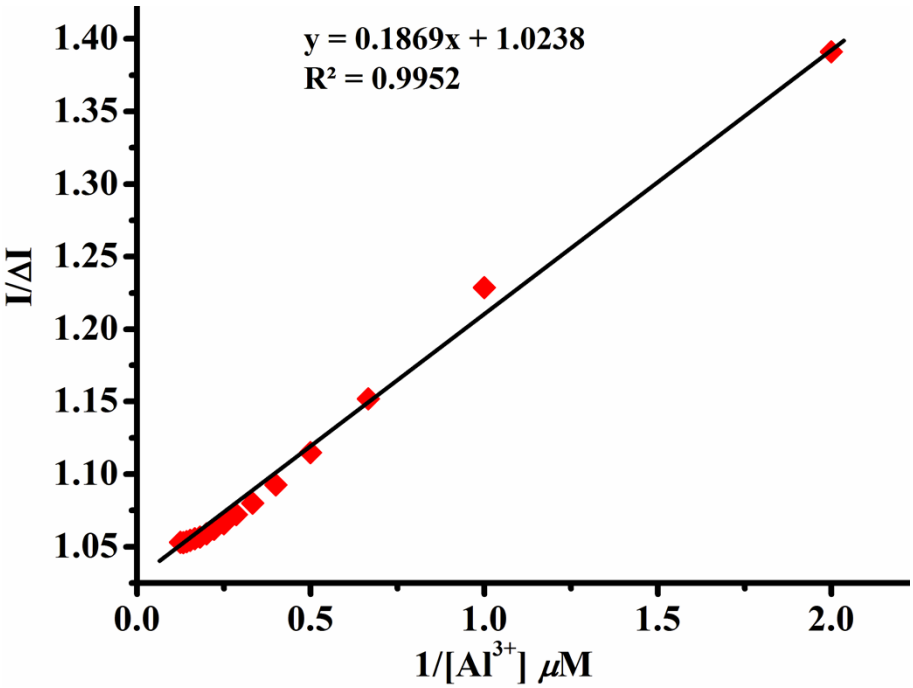

Fig. S12 Benesi Hildebrand plot for $\mathbf{H_3L}$ + Al^{3+} from the fluorescence spectral data considering 1:1 stoichiometry.

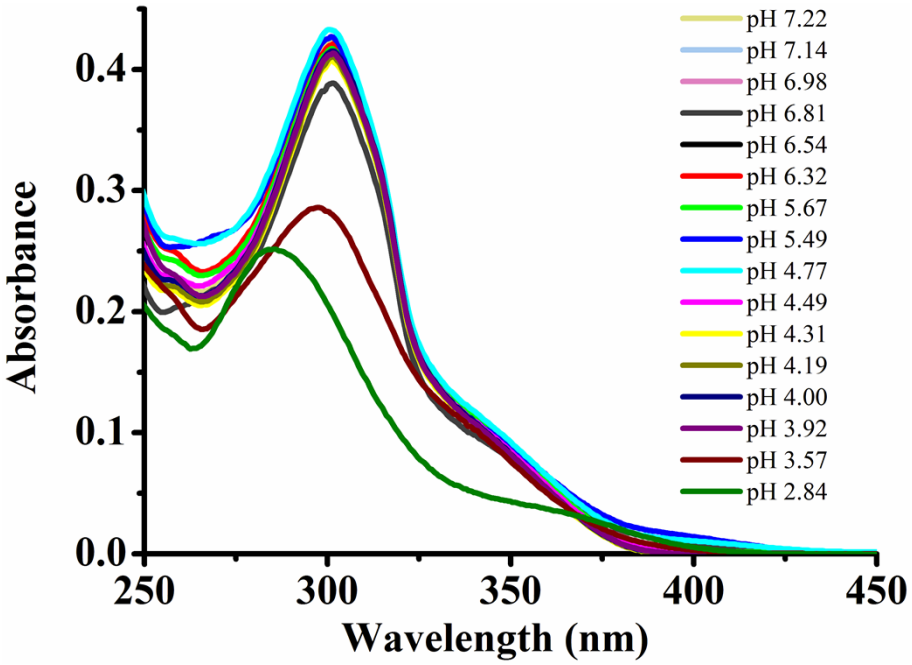

(a)

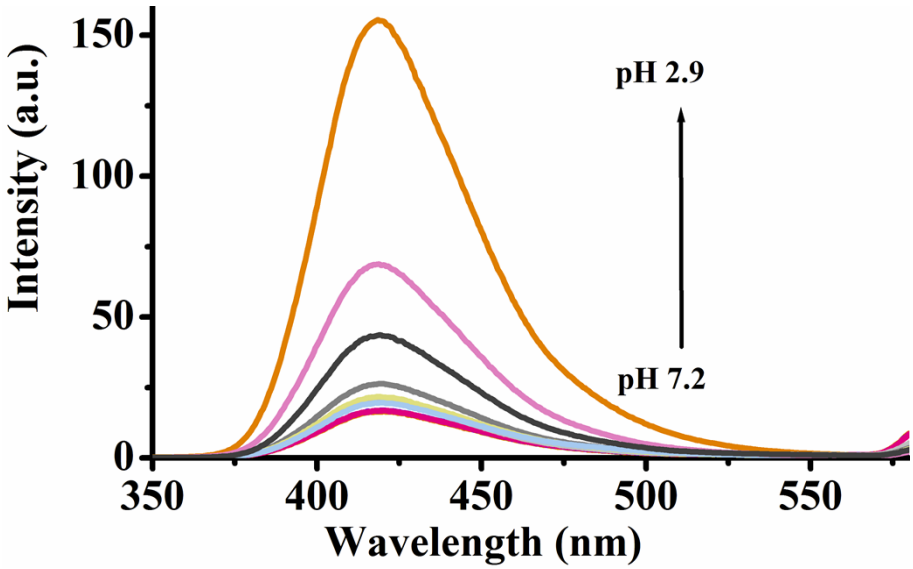

(b)

Fig. S13 (a) UV/vis and (b) Fluorescence experiments for **H_3L** with 0.1 M HCl solution to verify *p*H dependence. The experiment exhibited spectral changes which were ascribable to the deprotonation of **H_3L** but insignificant enough to pose any considerable interference in the detection of Al^{3+}/Cu^{2+}.

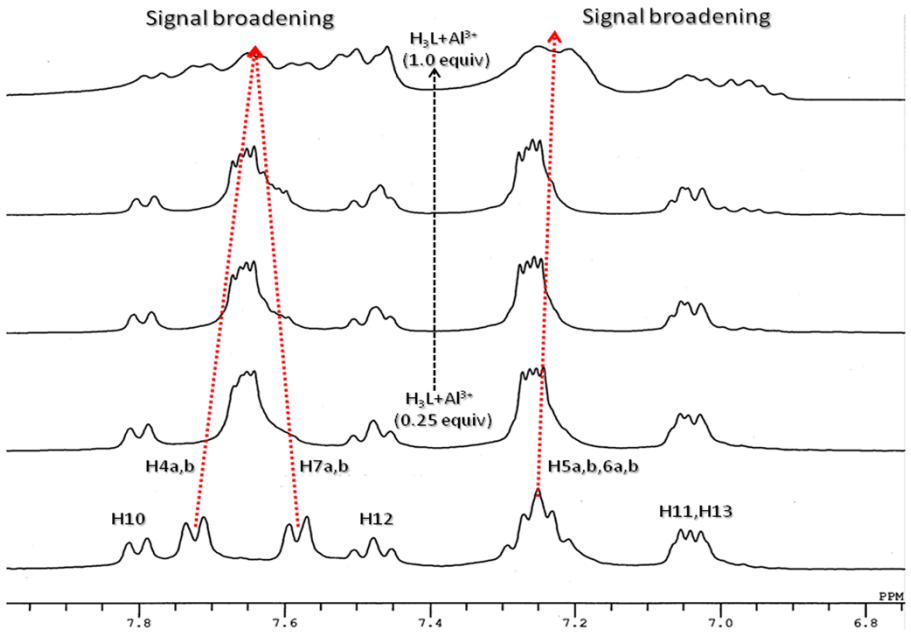

(a)

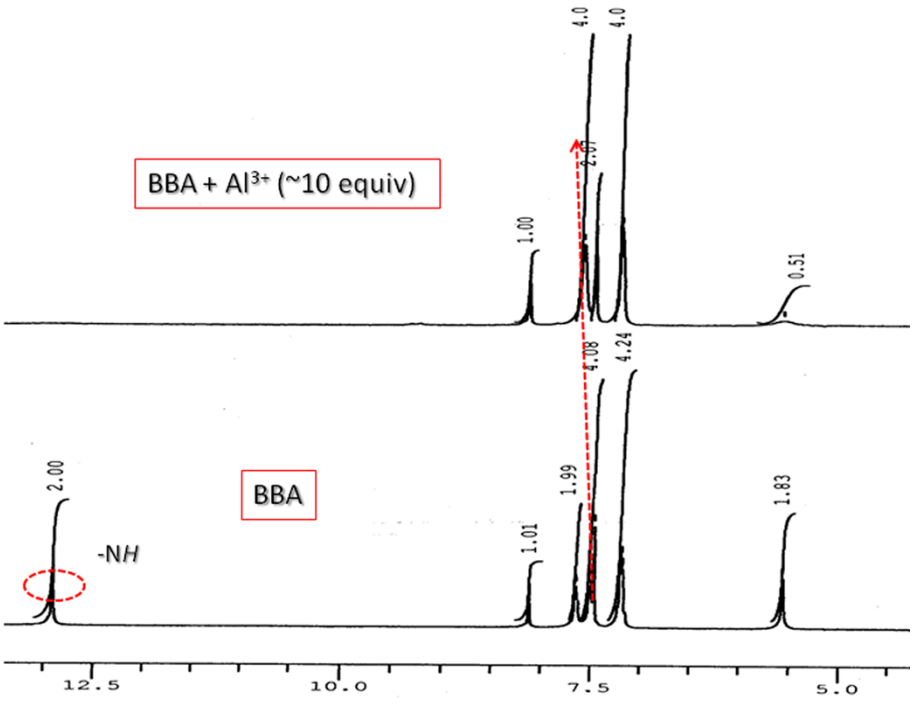

(b)

Fig. S14 (a) Partial ^{1}H NMR titration spectral overlay for **H_3L** *vs.* Al^{3+} showing significant chemical shifts for the benzimidazole protons. (b) ^{1}H NMR spectra for **BBA** showing significant shift of benzimidazole aromatic protons and complete disappearance of –NH signal in presence of Al^{3+}.

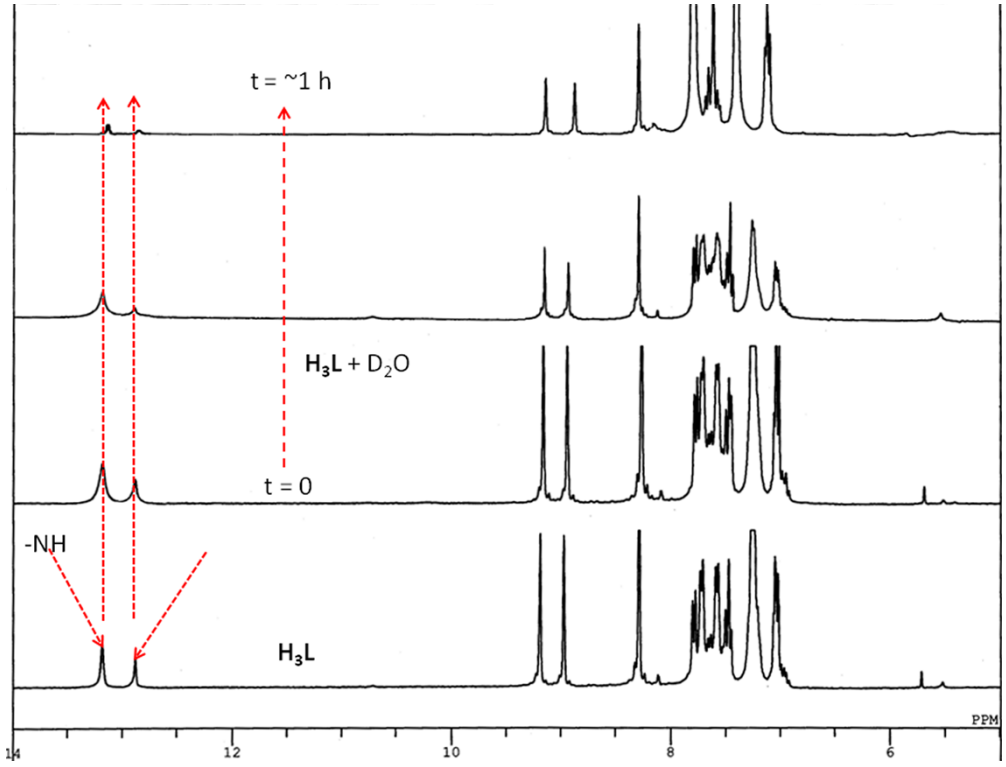

Fig. S15 ^{1}H NMR spectrum of **H_3L** only (dmso-d_6) and in presence of traces of blank **D_2O**.

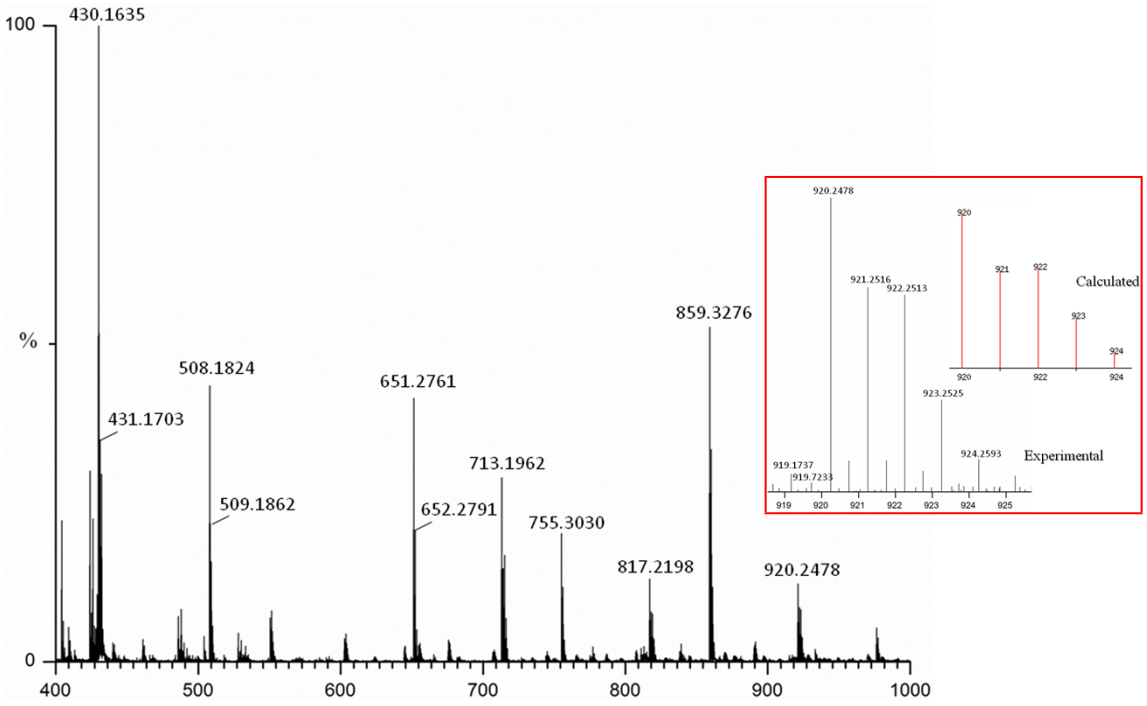
100
%
0
400
500
600
700
800
900
1000
430.1635
431.1703
508.1824
509.1862
651.2761
652.2791
713.1962
755.3030
817.2198
859.3276
920.2478
920.2478
921.2516
922.2513
923.2525
924.2593
919.1737
919.7233
Experimental
920
921
922
923
924
Calculated

(a)

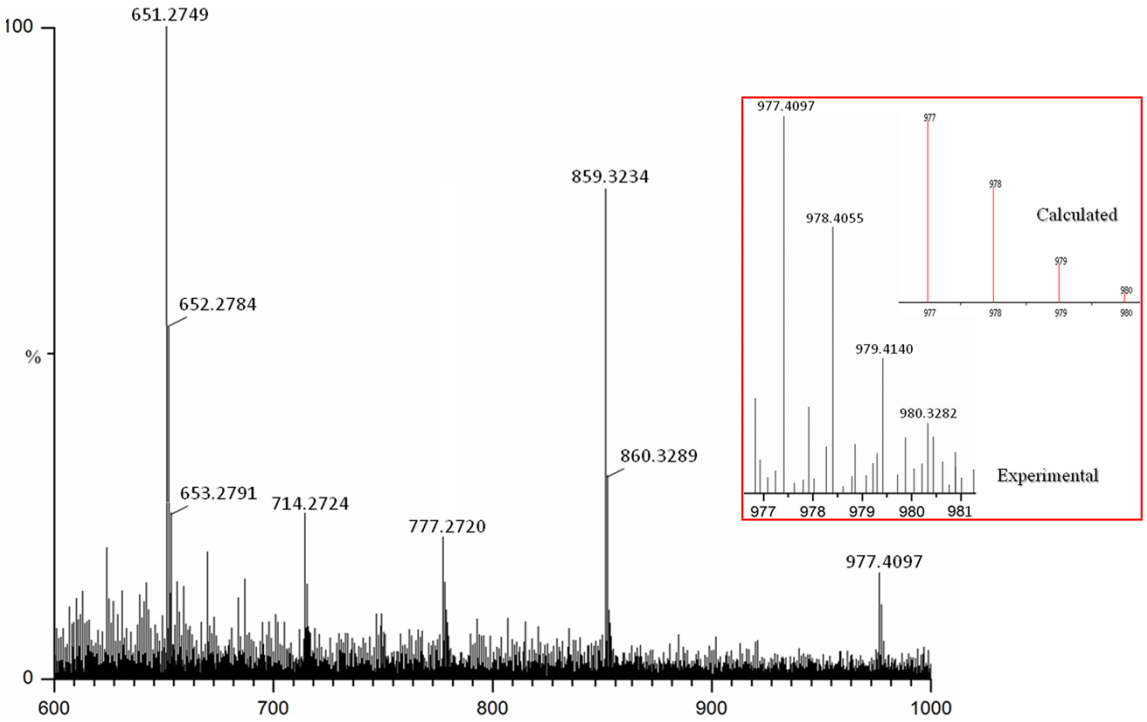
100
%
0
600
700
800
900
1000
651.2749
652.2784
653.2791
714.2724
777.2720
859.3234
860.3289
977.4097
977.4097
978.4055
979.4140
980.3282
Experimental
977
978
979
980
981
Calculated

(b)

Fig. S16 ESI-MS of (a) complex **1** and (b) complex **2**. These exhibit a good agreement with their relevant isotopic patterns on comparison with their respective calculated data (insets).

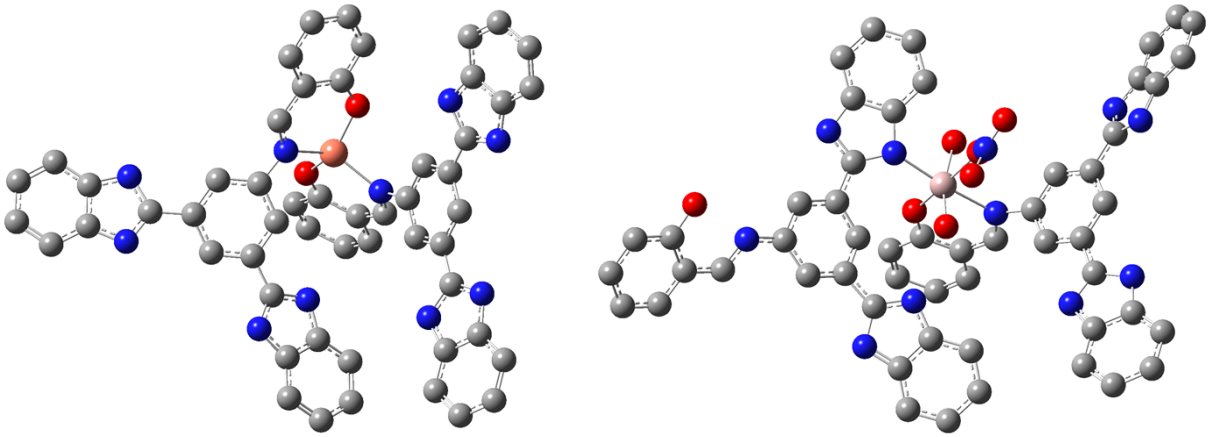

(a) (b)

Fig. S17 DFT optimized structures of (a) Cu^{II} –complex (**1**) and (b) Al^{III} –complex (**2**).

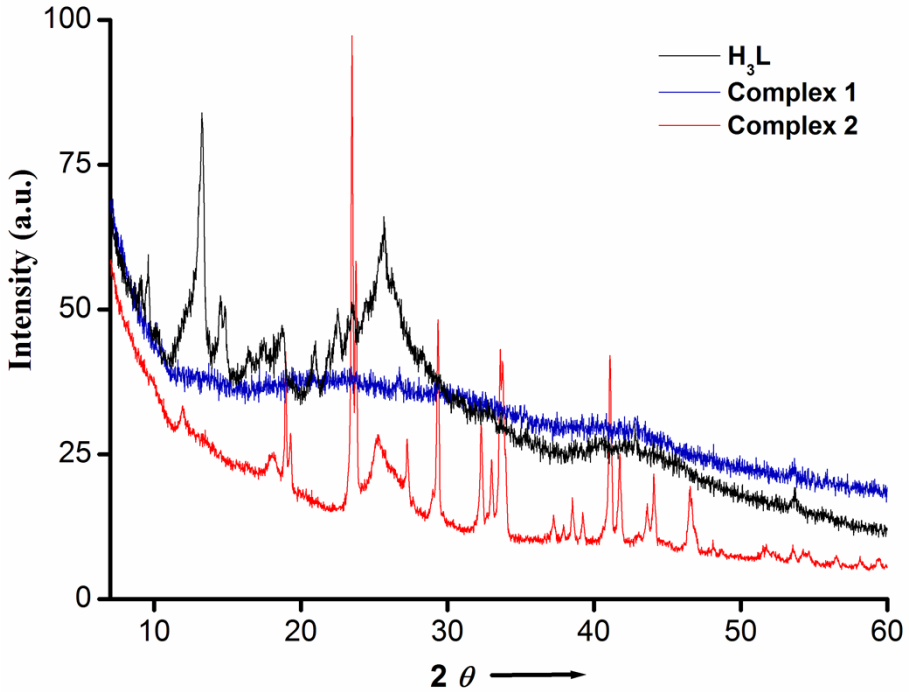

Fig. S18 Powder X-ray diffraction pattern of $\mathbf{H_3L}$, complex **1** ($\mathbf{H_3L}$ + Cu^{2+}) and complex **2** ($\mathbf{H_3L}$ + Al^{3+}). Diffractograms for **1** and **2** are quite different from $\mathbf{H_3L}$ substantiating the formations of respective complexes. However, peak intensity for **1** are very diminished

showing its amorphous nature however for 2, a well defined crystalline structure is signified provided that some in-situ generated metal-salts after drying cannot be ruled out in the PXRD pattern of **2**.[5]

Table S1. Bond Lengths (Å) and Angles (°) for **H_3L**.

N2—C5	1.357(4)	C10—C9	1.383(6)
N2—C11	1.377(5)	N3—C12	1.074(8)
N1—C5	1.313(4)	N3—C12^{i}	1.074(8)
N1—C6	1.395(4)	C9—C8	1.392(7)
C1—C2	1.392(4)	C12—C12^{i}	1.411(16)
C1—C2^{i}	1.392(4)	C12—C13	1.619(11)
C2—C3	1.395(4)	C12—O1	1.735(10)
C2—C5	1.470(4)	O2—C17	1.415(5)
C4—C3^{i}	1.395(4)	O1—C14	1.192(9)
C4—C3	1.395(4)	C16—C15^{i}	1.377(7)
C4—N3	1.393(7)	C16—C15	1.377(7)
C11—C10	1.385(5)	C15—C14	1.371(8)
C11—C6	1.407(5)	C14—C13	1.365(10)
C6—C7	1.397(5)	C13—C14^{i}	1.365(10)
C7—C8	1.371(6)	C13—C12^{i}	1.619(11)
C5—N2—C11	107.2(3)	C12—N3—C4	138.9(4)
C5—N1—C6	104.9(3)	C12^{i}—N3—C4	138.9(4)
C2—C1—C2^{i}	121.2(4)	C10—C9—C8	122.0(4)
C1—C2—C3	119.1(3)	C7—C8—C9	121.7(4)
C1—C2—C5	118.5(3)	N3—C12—C12^{i}	48.9(4)
C3—C2—C5	122.4(3)	N3—C12—C13	113.1(6)
C3^{i}—C4—C3	119.4(4)	C12^{i}—C12—C13	64.2(3)
C3^{i}—C4—N3	120.3(2)	N3—C12—O1	176.2(7)
C3—C4—N3	120.3(2)	C12^{i}—C12—O1	134.5(3)
C4—C3—C2	120.6(3)	C13—C12—O1	70.4(4)
N2—C11—C10	132.3(3)	C14—O1—C12	96.2(7)
N2—C11—C6	105.2(3)	C15^{i}—C16—C15	119.7(7)
C10—C11—C6	122.5(4)	C16—C15—C14	119.3(8)
N1—C5—N2	113.4(3)	O1—C14—C13	98.2(6)
N1—C5—C2	123.4(3)	O1—C14—C15	139.9(12)
N2—C5—C2	123.2(3)	C13—C14—C15	121.9(9)
N1—C6—C7	130.8(3)	C14^{i}—C13—C14	118.0(8)
N1—C6—C11	109.4(3)	C14^{i}—C13—C12^{i}	95.2(4)
C7—C6—C11	119.8(3)	C14—C13—C12^{i}	146.9(6)
C8—C7—C6	117.7(4)	C14^{i}—C13—C12	146.9(6)
C11—C10—C9	116.2(4)	C14—C13—C12	95.2(4)
C12—N3—C12^{i}	82.2(9)	C12^{i}—C13—C12	51.7(6)

Symmetry transformation used to generate equivalent atoms: 0.5-x, y, 1-z.

‘*i*’ has been used to indicate identical atoms

References

1. L. J. Bartolottiand and K. Fluchick, *In Reviews in Computational Chemistry*; K. B. Lipkowitz and D. Boyd, Ed. VCH: New York, 1996, **7**, 187.
2. (a) P. Hay and W. R. Wadt, *J. Chem. Phys*., 1985, **82**, 270; (b) W. R. Wadt and P. Hay, *J. Chem. Phys*., 1985, **82**, 284; (c) P. Hay and W. R. Wadt, *J. Chem. Phys*., 1985, **82**, 299.
3. M. J. Frisch, G. W. Trucks, H. B. Schlegel, G. E. Scuseria, M. A. Robb, J. R. Cheeseman, G. Scalmani, V. Barone, B. Mennucci, G. A. Petersson, H. Nakatsuji, M. Caricato, X. Li, H. P. Hratchian, A. F. Izmaylov, J. Bloino, G. Zheng, J. L. Sonnenberg, M. Hada, M. Ehara, K. Toyota, R. Fukuda, J. Hasegawa, M. Ishida, T. Nakajima, Y. Honda, O. Kitao, H. Nakai, T. Vreven, J. A. Montgomery, Jr., J. E. Peralta, F. Ogliaro, M. Bearpark, J. J. Heyd, E. Brothers, K. N. Kudin, V. N. Staroverov, R. Kobayashi, J. Normand, K. Raghavachari, A. Rendell, J. C. Burant, S. S. Iyengar, J. Tomasi, M. Cossi, N. Rega, J. M. Millam, M. Klene, J. E. Knox, J. B. Cross, V. Bakken, C. Adamo, J. Jaramillo, R. Gomperts, R. E. Stratmann, O. Yazyev, A. J. Austin, R. Cammi, C. Pomelli, J. W. Ochterski, R. L. Martin, K. Morokuma, V. G. Zakrzewski, G. A. Voth, P. Salvador, J. J. Dannenberg, S. Dapprich, A. D. Daniels, Ö. Farkas, J. B. Foresman, J. V. Ortiz, J. Cioslowski, and D. J. Fox, Gaussian 09, revision A.1, Gaussian, Inc., Wallingford, CT, 2009.
4. G. M. Sheldrick, *SHELXL-97, Program for X-ray Crystal Structure Refinement;* Göttingen University: Göttingen, Germany, 1997.
5. X.-F. Shen, Y.-S. Ding, J. C. Hanson, M. Aindow and S. L. Suib, *J. Am. Chem. Soc.,* 2006, **128**, 4570.